Research Article Vol. 4, No. 6 / June 2017 / Optica 643

Mid-infrared continuous-wave parametric amplification in chalcogenide microstructured fibers

Sida Xing,[1] Davide Grassani,[1] Svyatoslav Kharitonov,[1] Laurent Brilland,[2] Céline Caillaud,[2] Johann Trolès,[3] and Camille-Sophie Brès[1,*]

[1]Ecole Polytechnique Fédérale de Lausanne, Photonic Systems Laboratory (PHOSL), STI-IEL, Station 11, CH-1015 Lausanne, Switzerland
[2]SelenOptics, 57 rue de La Girolle, 35170 Bruz, France
[3]Equipe Verres et Céramiques, UMR-CNRS 6226, Institut des Sciences Chimiques de Rennes, Université de Rennes 1, 35042 Rennes, France
*Corresponding author: camille.bres@epfl.ch

Received 10 March 2017; revised 12 May 2017; accepted 16 May 2017 (Doc. ID 290479); published 13 June 2017

The persistent growth of interest in the middle infrared (MIR) is stimulating the development of sources and components. Novel waveguides and fibers for the efficient use of nonlinear effects in the MIR are being intensively studied. Highly nonlinear silica fibers have enabled record performances of highly versatile parametric processes in the telecommunication band. However, no waveguiding platforms (to our knowledge) have yet solved the trade-off among high nonlinearity, low propagation losses and dispersion in the MIR. As single waveguide designs have not yet hit this particular optimal point, only pulsed–pumped demonstrations have been carried out, hindering any application requiring narrow linewidth, continuous-wave (c.w.) operation, or signal modulation. Here, we show MIR c.w. parametric amplification in a $Ge_{10}As_{22}Se_{68}$ tapered fiber. Leveraging state-of-the-art fabrication techniques, we use a photonic crystal fiber (PCF) geometry combining high nonlinearity and low dispersion, while maintaining single mode and low losses in the short-wave IR and MIR. We experimentally demonstrate 5 dB signal amplification and 3 dB idler conversion efficiency using only 125 mW of pump in the 2 μm wavelength range. Our result is not only the first c.w. parametric amplification measured at 2 μm in any waveguide, but it also establishes GeAsSe PCF tapers as the most promising all-fibered, high-efficiency parametric converter for advanced applications in the MIR.

OCIS codes: (190.4380) Nonlinear optics, four-wave mixing; (190.4970) Parametric oscillators and amplifiers; (190.4370) Nonlinear optics, fibers; (060.2390) Fiber optics, infrared; (060.5295) Photonic crystal fibers.

https://doi.org/10.1364/OPTICA.4.000643

1. INTRODUCTION

The control of nonlinear processes in waveguides has long been a fruitful research area. In recent years, following the rapid progress of components and sources for the middle infrared (MIR), there has been increasing interest in the development of nonlinear waveguides and fibers for this specific spectral band. Parametric processes such as wavelength conversion and amplification based on four-wave mixing (FWM) are extremely versatile and useful. Compared with other MIR light generation/amplification techniques, parametric conversion in waveguides offers a compact, widely tunable, highly efficient solution operating at room temperature [1–3]. The efficiency of parametric processes depends on phase matching, the nonlinear strength, and losses. Waveguides have thus to be engineered taking into consideration material, geometry, and maturity of fabrication technology. Design requirements become even more stringent for continuous-wave (c.w.) pumping, which cannot benefit from the high peak powers of the pulsed regime and can result in thermal-related damages if the absorption is too high. Nevertheless, this regime is crucial for applications requiring c.w. light, narrow linewidth, or signal modulation, such as precise spectroscopy [4], free-space communication [5], and remote sensing [6].

Various nonlinear MIR platforms for parametric processes at 2 μm have been proposed in recent years, taking advantage of diode-pumped thulium or holmium doped silica fiber laser [7,8]. To reference their efficiency as a guideline for platform selection, we show in Table 1 the figure of merit (FOM) defined as the ratio of nonlinear coefficient γ to attenuation coefficient α [18]. Ideally this FOM should be as large as possible, highlighting the strong nonlinearity and low loss behavior of the nonlinear platform. Silica highly nonlinear fibers exhibit high absorption beyond 2 μm and a low γ, so their performance is poor in the MIR. Materials possessing both high nonlinear refractive indices (n_2) and good MIR transparency include soft glasses (tellurite and chalcogenide glasses) and silicon. Currently, platforms with the highest γ, such as silicon or As_2S_3 waveguides and chalcogenide

Table 1. Figure of Merit of Various Nonlinear Platforms Used for Parametric Processes at 2 μm

	n_2 (m^2/W)	n_2/α (m^3/W)	FOM (W^{-1})
SMF 28 [9,10]	$2.7 \cdot 10^{-20}$	$5.8 \cdot 10^{-18}$	0.19
Silica highly nonlinear fiber [10,11]	$2.7 \cdot 10^{-20}$	$1.6 \cdot 10^{-18}$	0.14
Si waveguide [12]	$1.1 \cdot 10^{-17}$	$1.9 \cdot 10^{-19}$	1.89
As_2S_3 waveguide[a] [13]	$3 \cdot 10^{-18}$	$2.6 \cdot 10^{-19}$	0.85
As_2Se_3 taper [14,15]	$1.1 \cdot 10^{-17}$	$1.6 \cdot 10^{-18}$	3.44
Tellurite SCF [16]	$5.9 \cdot 10^{-19}$	$8.6 \cdot 10^{-18}$	2.41
GeAsSe PCF [17]	$5.3 \cdot 10^{-18}$	$2.3 \cdot 10^{-17}$	7.31
GeAsSe PCF, tapered [this work]	$5.3 \cdot 10^{-18}$	$4.3 \cdot 10^{-17}$	85.05

[a]Values used are for 1550 nm.

step index tapers, exhibit high propagation losses. They are due to either sidewall scattering/surface smoothness and multiphonon absorption [1,12] or absorption in the polymer coating [14,19], significantly impacting their FOM. Soft glass suspended core fibers (SCFs) with low loss have been fabricated in recent years [16,20,21]. Due to the large refractive index difference, such SCFs are highly multimode, which both limits the amount of power effectively coupled to the fundamental mode and affects the phase matching condition of the parametric process [20]. The large air holes also allow an extended contact area with the atmosphere, such that strong water absorption and crystallization were found to severely degrade their nonlinear optical performance [22]. Photonic crystal fiber (PCF) structures are more promising thanks to possible single-mode behavior over a large wavelength span, better uniformity, and immunity to the environment [17], which allow very low propagation losses.

The strong normal material dispersion of chalcogenides, however, represents a major hurdle often translating into a trade-off among dispersion, losses, and multimode features. Here we overcome this trade-off by dispersion engineering a GeAsSe fiber through the combination of microstructuring and tapering. Chalcogenide PCFs for the MIR have been demonstrated previously, mostly targeting supercontinuum generation from pulsed pumps. Those PCFs typically have relatively large cores (around 10 μm), in order to reach light generation in the MIR. They leverage the inherently strong material nonlinearity of chalcogenides and are pumped deeper in the MIR to overcome the material dispersion barrier, while at the same time reducing losses. The tapering of step index fibers to increase nonlinearity while shaping dispersion has also been demonstrated. The zero-dispersion wavelength (ZDW) of such nanowires was successfully shifted to the thulium/holmium emission band (near 2 μm). However, the high core/cladding index contrast forces the fiber core to be tapered to a submicrometer diameter for single-mode pumping [23]. Nanowires are therefore coated with polymers to both give the necessary mechanical strength to the taper and compensate for the strong material dispersion [14,19], resulting in extremely high losses limiting the waveguide's effective length. Once again, only low-duty-cycle/high-peak-power pulsed sources were able to achieve amplification in this platform. A tapered chalcogenide PCF geometry was proposed in Ref. [24] for wavelength conversion in the telecom band. The main purpose was to increase the nonlinear parameter such that the resulting dispersion remained highly normal, leading to a very narrow conversion bandwidth, while the high losses at 1550 nm resulted in a low conversion efficiency (CE) of −30 dB.

In this work, we combine in a single fiber design all the necessary parameters for efficient c.w. parametric conversion, leading to a highly nonlinear platform that maintains single mode and low losses around 2 μm. In particular, we exploit the endlessly single-mode behavior dictated by the PCF structure [25] to maximize the coupled power on the fundamental mode and reduce modal interference. Moreover, light is confined to a structure entirely made of chalcogenide, which has reduced air interfaces and is unaffected by the polymer coating, leading to extremely low losses of 0.5 dB/m at 2 μm. The optimization of the design is reflected in its FOM. Finally, we leverage the degrees of freedom given by the PCF, tailoring the final core size and pitch-to-diameter ratio, to blueshift the ZDW in the neighborhood of the pump wavelength. This allows us to increase the interaction length while preserving a wide parametric bandwidth: we measure amplification over more than 10 nm at 1950 nm and a 3 dB conversion bandwidth of close to 20 nm at 2040 nm.

2. FIBER DESIGN AND FABRICATION

One of our design targets is to overcome the strong material dispersion of chalcogenide glass, which has a ZDW beyond 5 μm, while maintaining low losses and single mode. The ZDW of a PCF is highly dependent on the diameter-to-pitch ratio (ρ) [25]. For a given solid core diameter (ϕ), a large ρ value blueshifts the ZDW but also enhances the multimode behavior and fabrication difficulty of the fiber. Within the fabrication limits ($\rho < 0.6$) of GeAsSe PCF, solely varying ρ does not allow for a sufficient shift of the ZDW toward the 2 μm thulium/holmium band. Additional reduction of the core size is necessary to strengthen the waveguide dispersion. Tapering is an efficient way to reduce the fiber waist size to values not easily accessible with direct fabrication [Fig. 1(a)] while maintaining the initial ratio. The designed fiber was thus fabricated via a two-step method. First, a GeAsSe PCF featuring three rings of holes aiming at $\rho \approx 0.6$ and $\phi_s \approx 4$ μm was fabricated [Fig. 1(b)]. This combination of material and geometry was selected for three reasons, mainly related to fabrication: (1) the small initial core facilitates the tapering step, (2) GeAsSe allows for the reduction of the core size without excess loss, and (3) it has a lower material dispersion with respect to AsSe compounds [26]. The central part of the fiber

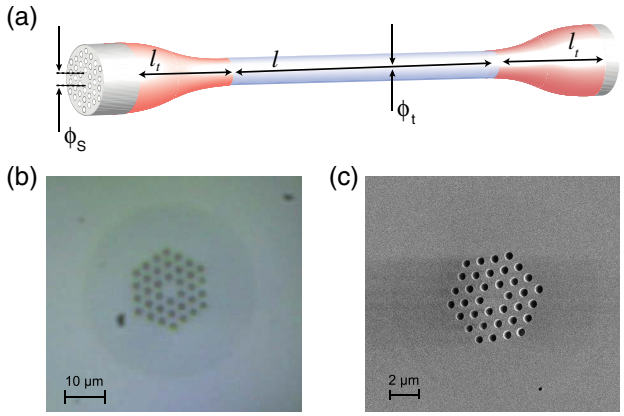

Fig. 1. Dispersion engineered GeAsSe tapered PCF. (a) Schematic of the GeAsSe fiber, (b) optical microscope image of the microstructured fiber before tapering, and (c) scanning electron microscope image after tapering, within the waist. The structure appears well preserved.

was then tapered to achieve a core diameter of about $\phi_t = 1.5$ μm [Fig. 1(c)] and length $l \approx 1$ m, between two transition regions of length $l_t \approx 1.5$ cm.

The fabrication starts from a previously synthesized highly purified $Ge_{10}As_{22}Se_{68}$ bulk glass. The glass has an optical loss of 0.6 dB/m measured at 1.55 μm. Part of the GeAsSe glass was then molded to fabricate a preform with three hexagonal rings of air holes [27]. The preform was drawn into a cane with a 4 mm diameter. This cane was then inserted into an As_2Se_3 tube, and the whole tube assembly was drawn into a PCF with an outer diameter of approximately 130 μm and a core size of about 4 μm. The pitch distance, Λ, was measured to be approximately 2.88 μm, and the air hole diameter was 1.69 μm, leading to a diameter-to-pitch ratio of 0.58. The propagation loss of the PCF was measured to be 0.65 dB/m at 1.55 μm from a cutback experiment with 2.5 m of the fabricated PCF. Using a segment of this PCF, several tapered fibers with a length ranging from 0.7 m to 1 m were then fabricated on the drawing tower at a temperature of around 270°C. Longer fibers with low loss and high uniformity are still challenging to obtain.

3. EXPERIMENTAL SETUP

The all-fibered FWM setup is detailed in Fig. 2. The 2 μm pump and signal lasers used in this experiment are custom built Tm-doped fiber lasers [9]. The pump wavelength was selected discretely with various fiber Bragg gratings, while the signal wavelength was selected by a tunable bandpass grating filter with a 1 nm linewidth. Both configurations were checked using a photodetector to confirm the absence of pulsing operation. We measured the pump laser linewidth to be less than 0.08 nm at 1950 nm, limited by the resolution of our optical spectrum analyzer (OSA). The output from the pump and signal lasers was combined by a 95/5 fiber coupler, designed for operating at 2 μm, and then sent through a circulator to prevent back-reflection. A fibered polarization beam splitter was mounted after the circulator with one arm connected to a polarization-maintaining (PM) lensed fiber for coupling into the PCF. The other arm was used for power monitoring. We collected the output from the chalcogenide fiber by using another PM lensed fiber, subsequently sent to the OSA (Yokogawa AQ 6375). A total insertion loss of 8.5 dB was measured at 1950 nm, where approximately 4.5 dB was the total coupling loss, 3.4 dB from the transition regions and 0.6 dB from the propagation loss (α) through a tapered region length of 1.2 m.

We used an interferometric method [9] to characterize the dispersion of the untapered PCF. However, the phase delay contribution from the untapered and transition sections hinders this technique from directly yielding a reliable dispersion measurement of the tapered PCF. The FWM process, at the basis of parametric amplification and frequency conversion, can also be used to retrieve the dispersion, giving a good indication of the fiber uniformity, suppression of the higher-order modes, and strength of the birefringence in the tapered region.

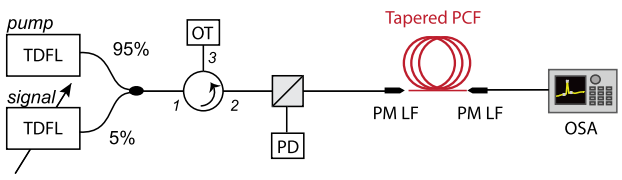

Fig. 2. Experimental setup. TDFL, thulium-doped fiber laser; OT, optical terminator; PD, photodiode; PM LF, polarization-maintaining lensed fiber; OSA, optical spectrum analyzer.

4. EXPERIMENTAL RESULTS AND ANALYSIS

We first used the commercial finite element method software COMSOL to simulate the PCF's propagation constant and numerically derive the group velocity dispersion (GVD). The simulation indicates that the fiber is slightly multimode at 2 μm. However, the effective index of higher-order modes is very close to the effective index of the cladding. Thus, due to the large wave vector mismatch between the fundamental and high-order modes, in practice, only the fundamental mode is excited [28]. To confirm the simulated GVD and effective single-mode behavior, we measured the dispersion of the untapered 4 μm core PCF using a white light interferometric technique. Excellent agreement with theory, as can be seen in Fig. 3(a), indicates the accuracy of our model, effective single-mode operation, and quality of the fiber. As expected, the dispersion is strongly normal at 2 μm, with a ZDW located near 2.9 μm. From this model, further simulations were performed to determine the target waist core size, resulting in $\phi_t = 1.5$ μm. The simulated dispersion of the tapered fiber is shown in Fig. 3(a), with the shaded area representing possible birefringence and other fabrication imperfections leading to a 2% of ρ fluctuation over the ∼1 m tapered region. The ZDW of the tapered PCF is expected to be between 2.1 and 2.2 μm, depending on the input laser polarization and fabricated ratio.

The parametric behavior of the tapered fiber was studied by FWM using a c.w. pump together with a c.w. signal. To reduce the impact of other nonlinear effects, all characterizations were performed at a low pump power level (<20 mW at the fiber waist). The idler waves show well-defined phase matching features, confirming the uniformity, single-mode nature, and low loss of the taper [see Fig. 3(b)]. The nonlinear Schrodinger equation was then used to fit the CE data to retrieve the fiber parameters:

$$i\frac{\partial}{\partial z}A(z,t) + \frac{i\alpha}{2}A - \frac{\beta_2}{2}\frac{\partial^2 A}{\partial t^2} + \gamma|A|^2A = 0. \quad (1)$$

In the above equation, $A(z,t)$ is the electric field amplitude, β_2 is the GVD, and α is the linear propagation loss. We consider $A(z,t)$ as an ideal single-wavelength laser, such that the fitting can be used to corroborate the c.w. operation of the fiber lasers. The nonlinear coefficient γ of the tapered PCF was retrieved to be $\gamma \approx 10\ \mathrm{W^{-1}\,m^{-1}}$, in agreement with the value calculated using the measured n_2 from our previous work [17] and the effective area A_{eff} simulated with COMSOL. The tolerance of this fitting was set to 0.05 nm, i.e., the resolution of the OSA. The contribution of parametric conversion in the untapered region of the input side was also added in the simulated result of the tapered fibers. Since the 1.5 cm taper transition regions are significantly shorter than the taper length, we neglected their contribution during the simulation. The larger effective area and the shorter length of the untapered sections result in a slight rise in the magnitude of the CE minima, without changing their positions. We extracted the dispersion parameter β_2 of the waist region for pump wavelengths at 1950, 1980, 2008, and 2040 nm, while the signal was tuned over 100 nm in the 2 μm range. We also characterized different tapered fibers, with waist lengths ranging from 0.8 to

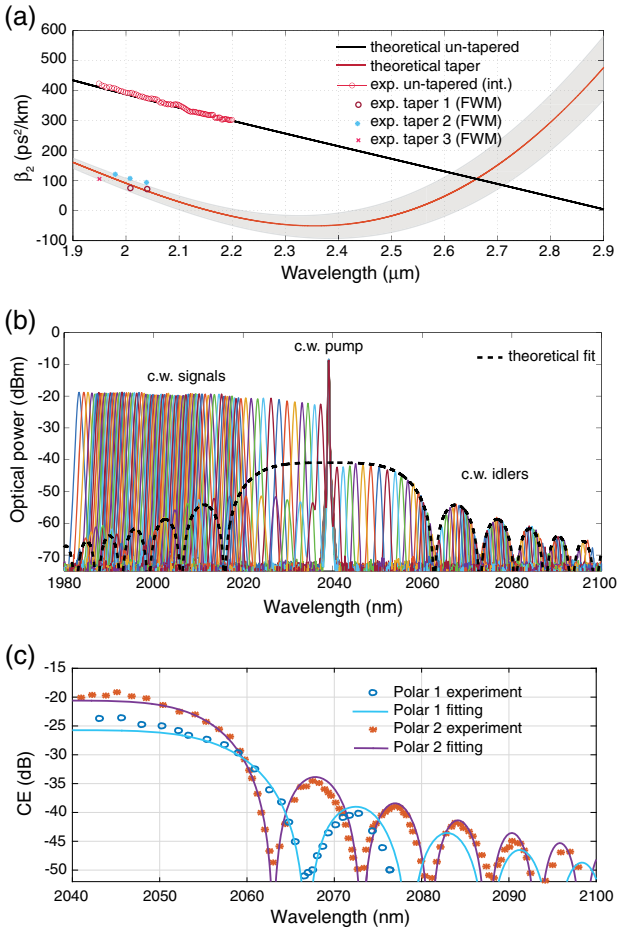

Fig. 3. Engineered GeAsSe microstructured taper characteristics. (a) Dispersion of the untapered and tapered fiber obtained from simulations (solid lines). Measured dispersion on the fabricated fibers obtained from interferometric measurements (int.) and four-wave mixing data (FWM) are also plotted. (b) Example of FWM spectra at the output of the tapered fiber for a c.w. pump positioned at 2040 nm with 13 mW coupled power. The data are in excellent agreement with the theoretical fitting. (c) Fitting of the experimental CE points for a 78 cm long tapered fiber at 2040 nm pump; rotating the input lensed fiber revealed its birefringence.

1.3 m, fabricated using the same fiber spool. The experimental values for all fibers are in excellent agreement with the predicted dispersion [Fig. 3(a)]. An example of FWM spectra and relative theoretical fit for a 2040 nm pump with 13 mW of coupled pump power and approximately 1 mW of coupled signal power is shown in Fig. 3(b).

We also experimentally investigated the fiber birefringence. An ideal hexagonal PCF is not birefringent [29]; however, the symmetry of real PCF is always broken due to fabrication imperfections. Slight variations in the cladding air hole size lead to different diameter-to-pitch ratios depending on the input light polarization. We checked the fiber birefringence experimentally at 2040 nm by rotating the angle of input PM lensed fiber. The recorded FWM spectra were converted as CE versus signal detuning curves. We found the effective fast and slow axes of this fiber, shown in Fig. 3(c), which clearly show the fiber is birefringent. This polarization-dependent dispersion corresponds to the fluctuation of ρ between 0.58 and 0.585, further proving the good uniformity of the tapered PCF. The difference in CE is due to a 2 dB lower coupling efficiency on polarization 1.

The combination of high γ and long effective length leads to the amplification of the laser amplified spontaneous emission, as depicted in Fig. 4(a) for a 1950 nm pump. Phase matching features emerge from the OSA noise floor with increasing pump power. With only 125 mW pump coupled power, signal amplification and cascaded FWM up to 3 orders were observed while maintaining the initial linewidth of the signal and on the corresponding idler of approximately 0.3 nm.

The CE is plotted in Fig. 4(b) as a function of idler wavelength for 125 mW coupled pump at 1950 nm, while the on/off amplification on the signal for different coupled pump powers is plotted in Fig. 4(c). Operation above transparency is observed near the pump with a −20 dB bandwidth of 15 nm, while we recorded close to 5 dB of signal amplification. In Fig. 4(c), a reduction of the amplification bandwidth can be seen with

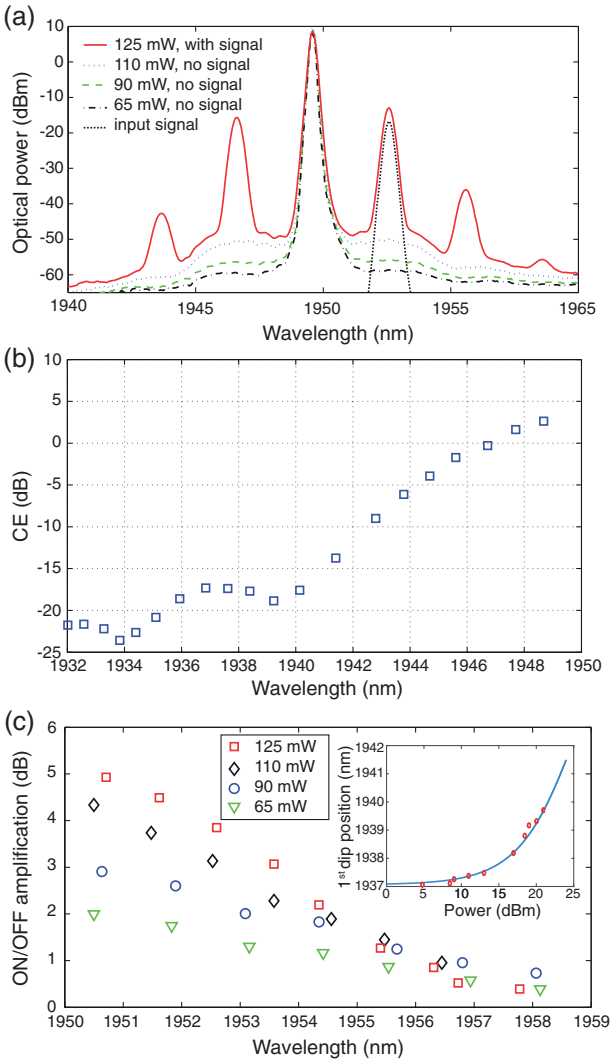

Fig. 4. Experimental characterization of a 1.2 m long taper for 1950 nm pump. (a) Output spectra for 65, 90, and 110 mW coupled pump powers, and 125 mW with a 1 mW signal. Cascaded FWM is observed. (b) CE as a function of idler wavelength for 125 mW pump power at 1950 nm, (c) ON/OFF signal amplification for four coupled pump powers. Inset: experimentally measured and simulated positions of the CE's first dip as a function of coupled pump power.

increasing pump power. This behavior is due to the nonlinear contribution to the phase mismatch, as the pump is located in the normal dispersion regime. To quantify the effect of nonlinear phase contribution, and for comparison with theory, we also plotted the theoretical position of the first dip as a function of the pump power [inset of Fig. 4(c)]. A perfect matching with the theory indicates a good estimation of linear and nonlinear phase mismatch and confirms no change in the fiber geometry even at the highest pump power.

The input–output characteristics of the tapered fiber pumped at 1950 nm were further examined with a signal at 1952 nm. The CE as a function of pump power is plotted in Fig. 5(a). The fitted experimental data exhibit a slope of approximately 1.8 with no onset of saturation. In the undepleted pump approximation, we expect a quadratic relation between pump and idler. This small discrepancy in our experiment comes from the cascaded FWM [shown in Fig. 4(a)] when the idler acts as a pump and is depleted due to the high power of the pump, which now acts as the signal. It is also worth noting that our results establish the excellent power handling of the chalcogenide fiber in the MIR. For almost 20 years, the c.w. power handling of chalcogenide fibers has been an important concern. It was believed that intensities were limited to the order of kW/cm^2 [30,31], greatly hindering the potential of this extremely nonlinear and high-viscosity [31] MIR glass material. Recently, based on the parameters provided in Ref. [32], a step-indexed As_2S_3 fiber tested with a thulium-doped fiber laser at 1.97 μm was found to handle 5.6 MW/cm^2. Here we confirm this finding with an even higher laser intensity of at least 6.62 MW/cm^2 (for the 125 mW power). Also, shown in Fig. 5(a) is the relationship between input and output pump power, as monitored on the OSA: the linear fit indicates constant fiber losses and stable coupling.

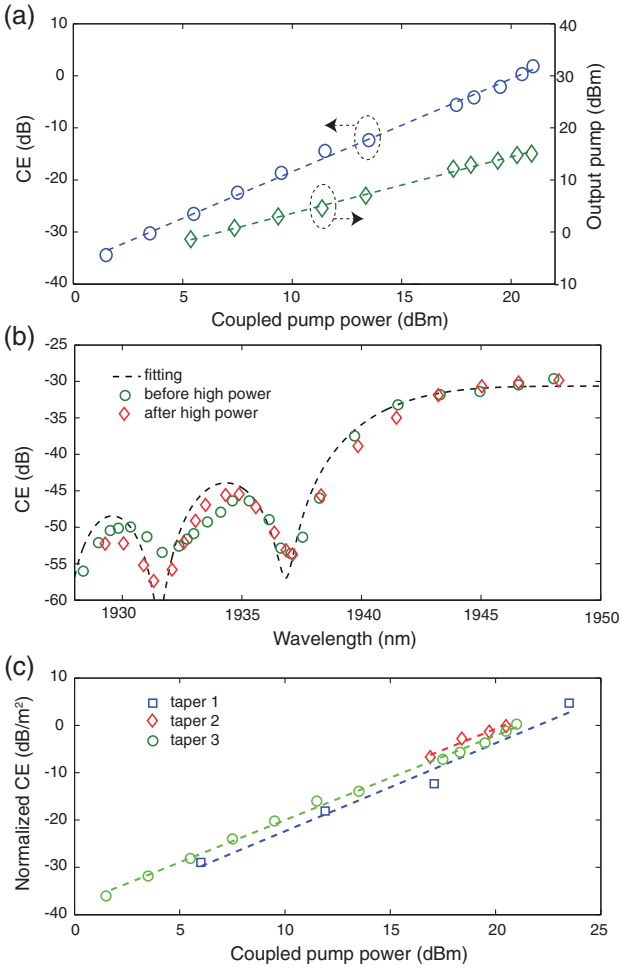

Fig. 5. Mid-IR parametric amplifier performance and repeatability. (a) CE as a function of coupled pump power for a 1950 nm pump and a 1952 nm signal. Output pump power as a function of coupled pump power is also plotted. (b) CE as a function of wavelength for a 3 mW pump before and after high power (125 mW) testing, (c) normalized CE in decibels per length squared (dB/m^2) as a function of coupled pump power for three different tapers obtained from the same fiber. Note that taper 1 was tested at 1980 nm instead of 1950 nm.

To further confirm that no irreversible structural damage was induced during the experiments, the fiber was recharacterized right after the highest employed power (125 mW), with 3 mW of coupled pump. The parametric behavior of the fiber remained identical, as seen in Fig. 5(b), while no structural or loss changes were observed.

To check the repeatability of the results, we characterized two additional tapered PCFs with identical geometry (length of 0.8 and 1.2 m). All three tapers reported here were fabricated from the same fiber spool and have similar linear transmission loss (<0.2 dB difference). Since the length of the three tapers differs slightly, CE over length squared is plotted as a function of coupled pump power in Fig. 5(c). CE transparency and signal amplification were observed in all tapers, even at different pump wavelengths, confirming the repeatability of the experiment and of the taper features. The slight discrepancies are due to small loss variations in the taper transition region. To reach higher amplification values, the pump power was increased, leading to fiber damage. The damage is not due to power handling limitations, but rather to a fiber fuse from a localized defect, likely caused by microbending or local damage during the polymer coating process. (See Supplement 1.) It should be noted that fiber fuse has been observed in silica fibers for the same order of power densities (the MW/cm^2 range).

5. CONCLUSIONS

In summary, we presented wavelength conversion above transparency and parametric amplification at 2 μm using low c.w. pumping power and relatively short fibers. The engineered GeAsSe PCF taper combines in a single design low dispersion (ZDW near 2.1 μm), a high γ of 10 W^{-1} m^{-1}, single-mode behavior, and low loss of 0.5 dB/m. We measured up to 5 dB of amplification with only 125 mW of power inside the waist region. The samples show excellent power handling capabilities, answering persistent doubts about c.w. operation in chalcogenide fibers. Moreover, they can be spliced with silica fibers [32], enabling compatibility with current fiber-based devices and reducing coupling losses. However, proper handling and protection of such fibers, especially from water absorption, is important to guarantee good aging performance [33]. Improvement in fabrication techniques, longer fiber, and a better polymer protection layer process (see Supplement 1) will lead to better CE and signal amplification. The wavelength-dependent loss of GeAsSe [33] shows absolutely no obstacles to pumping at the ZDW or slightly in the anomalous regime, which would further increase CE and bandwidth. We believe that these results pave the way for fully fibered optical

processing devices based on parametric processes for the MIR range operating on low c.w. power.

Funding. H2020 European Research Council (ERC) (ERC-2012- StG 306630-MATISSE).

Acknowledgment. The authors are thankful to Adrien Billat from the Photonics Systems Laboratory, École Polytechnique Fédérale de Lausanne, for taking the scanning electron microscope images of the fiber.

See Supplement 1 for supporting content.

REFERENCES

1. S. Zlatanovic, J. S. Park, S. Moro, J. M. C. Boggio, I. B. Divliansky, N. Alic, S. Mookherjea, and S. Radic, "Mid-infrared wavelength conversion in silicon waveguides using ultracompact telecom-band-derived pump source," Nat. Photonics **4**, 561–564 (2010).
2. R. K. W. Lau, M. Ménard, Y. Okawachi, M. A. Foster, A. C. Turner-Foster, R. Salem, M. Lipson, and A. L. Gaeta, "Continuous-wave mid-infrared frequency conversion in silicon nanowaveguides," Opt. Lett. **36**, 1263–1265 (2011).
3. X. Liu, B. Kuyken, G. Roelkens, R. Baets, R. M. Osgood, and W. M. J. Green, "Bridging the mid-infrared-to-telecom gap with silicon nanophotonic spectral translation," Nat. Photonics **6**, 667–671 (2012).
4. G. Wysocki, R. Lewicki, R. F. Curl, F. K. Tittel, L. Diehl, F. Capasso, M. Troccoli, G. Hofler, D. Bour, S. Corzine, R. Maulini, M. Giovannini, and J. Faist, "Widely tunable mode-hop free external cavity quantum cascade lasers for high resolution spectroscopy and chemical sensing," Appl. Phys. B **92**, 305–311 (2008).
5. E. Luzhansky, F.-S. Choa, S. Merritt, A. Yu, and M. Krainak, "Mid-IR free-space optical communication with quantum cascade lasers," Proc. SPIE **9465**, 946512 (2015).
6. S. Kameyama, M. Imaki, Y. Hirano, S. Ueno, S. Kawakami, D. Sakaizawa, and M. Nakajima, "Development of 1.6 μm continuous-wave modulation hard-target differential absorption lidar system for CO_2 sensing," Opt. Lett. **34**, 1513–1515 (2009).
7. N. Simakov, A. Hemming, W. A. Clarkson, J. Haub, and A. Carter, "A cladding-pumped, tunable holmium doped fiber laser," Opt. Express **21**, 28415–28422 (2013).
8. J. Li, Z. Sun, H. Luo, Z. Yan, K. Zhou, Y. Liu, and L. Zhang, "Wide wavelength selectable all-fiber thulium doped fiber laser between 1925 nm and 2200 nm," Opt. Express **22**, 5387–5399 (2014).
9. S. Kharitonov, A. Billat, and C.-S. Brès, "Kerr nonlinearity and dispersion characterization of core-pumped thulium-doped fiber at 2 μm," Opt. Lett. **41**, 3173–3176 (2016).
10. D. Milam and M. J. Weber, "Measurement of nonlinear refractive-index coefficients using time-resolved interferometry: application to optical materials for high-power neodymium lasers," J. Appl. Phys. **47**, 2497–2501 (1976).
11. A. Gershikov, E. Shumakher, A. Willinger, and G. Eisenstein, "Fiber parametric oscillator for the 2 μm wavelength range based on narrowband optical parametric amplification," Opt. Lett. **35**, 3198–3200 (2010).
12. X. Liu, R. M. Osgood, Y. A. Vlasov, and W. M. J. Green, "Mid-infrared optical parametric amplifier using silicon nanophotonic waveguides," Nat. Photonics **4**, 557–560 (2010).
13. M. R. E. Lamont, B. Luther-Davies, D.-Y. Choi, S. Madden, X. Gai, and B. J. Eggleton, "Net-gain from a parametric amplifier on a chalcogenide optical chip," Opt. Express **16**, 20374–20381 (2008).
14. N. Abdukerim, L. Li, and M. Rochette, "Chalcogenide-based optical parametric oscillator at 2 μm," Opt. Lett. **41**, 4364–4367 (2016).
15. G. Lenz, J. Zimmermann, T. Katsufuji, M. E. Lines, H. Y. Hwang, S. Spälter, R. E. Slusher, S. W. Cheong, J. S. Sanghera, and I. D. Aggarwal, "Large Kerr effect in bulk Se-based chalcogenide glasses," Opt. Lett. **25**, 254–256 (2000).
16. T. Cheng, L. Zhang, X. Xue, D. Deng, T. Suzuki, and Y. Ohishi, "Broadband cascaded four-wave mixing and supercontinuum generation in a tellurite microstructured optical fiber pumped at 2 μm," Opt. Express **23**, 4125–4134 (2015).
17. S. Xing, D. Grassani, S. Kharitonov, A. Billat, and C.-S. Brès, "Characterization and modeling of microstructured chalcogenide fibers for efficient mid-infrared wavelength conversion," Opt. Express **24**, 9741–9750 (2016).
18. M. E. Marhic, P. A. Andrekson, P. Petropoulos, S. Radic, C. Peucheret, and M. Jazayerifar, "Fiber optical parametric amplifiers in optical communication systems," Laser Photon. Rev. **9**, 50–74 (2015).
19. R. Ahmad and M. Rochette, "High efficiency and ultra broadband optical parametric four-wave mixing in chalcogenide-PMMA hybrid microwires," Opt. Express **20**, 9572–9580 (2012).
20. S. D. Le, D. M. Nguyen, M. Thual, L. Bramerie, M. Costa e Silva, K. Lenglé, M. Gay, T. Chartier, L. Brilland, D. Méchin, P. Toupin, and J. Troles, "Efficient four-wave mixing in an ultra-highly nonlinear suspended-core chalcogenide $As_{38}Se_{62}$ fiber," Opt. Express **19**, B653–B660 (2011).
21. I. Savelii, O. Mouawad, J. Fatome, B. Kibler, F. Désévédavy, G. Gadret, J. C. Jules, P. Y. Bony, H. Kawashima, W. Gao, T. Kohoutek, T. Suzuki, Y. Ohishi, and F. Smektala, "Mid-infrared 2000-nm bandwidth supercontinuum generation in suspended-core microstructured sulfide and tellurite optical fibers," Opt. Express **20**, 27083–27093 (2012).
22. O. Mouawad, F. Amrani, B. Kibler, J. Picot-Clémente, C. Strutynski, J. Fatome, F. Désévédavy, G. Gadret, J. C. Jules, O. Heintz, E. Lesniewska, and F. Smektala, "Impact of optical and structural aging in As_2S_3 microstructured optical fibers on mid-infrared supercontinuum generation," Opt. Express **22**, 23912–23919 (2014).
23. C. Baker and M. Rochette, "High nonlinearity and single-mode transmission in tapered multimode As_2Se_3-PMMA fibers," IEEE Photon. J. **4**, 960–969 (2012).
24. S. D. Le, M. Gay, L. Bramerie, M. Costa e Silva, K. Lenglé, T. Chartier, M. Thual, J.-C. Simon, L. Brilland, D. Méchin, P. Toupin, and J. Troles, "Wavelength conversion in a highly nonlinear chalcogenide microstructured fiber," Opt. Lett. **37**, 4576–4578 (2012).
25. P. St. J. Russell, "Photonic-crystal fibers," J. Lightwave Technol. **24**, 4729–4749 (2006).
26. P. Toupin, L. Brilland, J. Trolès, and J.-L. Adam, "Small core Ge-As-Se microstructured optical fiber with single-mode propagation and low optical losses," Opt. Mater. Express **2**, 1359–1366 (2012).
27. Q. Coulombier, L. Brilland, P. Houizot, T. Chartier, T. N. N'Guyen, F. Smektala, G. Renversez, A. Monteville, D. Méchin, T. Pain, H. Orain, J.-C. Sangleboeuf, and J. Trolès, "Casting method for producing low-loss chalcogenide microstructured optical fibers," Opt. Express **18**, 9107–9112 (2010).
28. J. M. Dudley, G. Genty, and S. Coen, "Supercontinuum generation in photonic crystal fiber," Rev. Mod. Phys. **78**, 1135–1184 (2006).
29. M. J. Steel, T. P. White, C. M. de Sterke, R. C. McPhedran, and L. C. Botten, "Symmetry and degeneracy in microstructured optical fibers," Opt. Lett. **26**, 488–490 (2001).
30. J. S. Sanghera and I. D. Aggarwal, "Active and passive chalcogenide glass optical fibers for IR applications: a review," J. Non-Cryst. Solids **256**, 6–16 (1999).
31. G. M. Tao, H. Ebendorff-Heidepriem, A. M. Stolyarov, S. Danto, J. V. Badding, Y. Fink, J. Ballato, and A. F. Abouraddy, "Infrared fibers," Adv. Opt. Photon. **7**, 379–458 (2015).
32. R. Thapa, R. R. Gattass, V. Nguyen, G. Chin, D. Gibson, W. Kim, L. B. Shaw, and J. S. Sanghera, "Low-loss, robust fusion splicing of silica to chalcogenide fiber for integrated mid-infrared laser technology development," Opt. Lett. **40**, 5074–5077 (2015).
33. P. Toupin, L. Brilland, D. Méchin, J.-L. Adam, and J. Troles, "Optical aging of chalcogenide microstructured optical fibers," J. Lightwave Technol. **32**, 2428–2432 (2014).